



# Deep learning-based approach in surface thermography for inverse estimation of breast tumor size

Zakaryae Khomsi<sup>\*</sup>, Mohamed Elfezazi, Larbi Bellarbi

ENSAM-ENSIAS, ST2I Laboratory, E2SN Team, Mohammed V University in Rabat, Morocco

## ARTICLE INFO

Editor: DR B Gyampoh

**Keywords:**

Inverse bio-heat problem  
Breast cancer modeling  
Synthetic data  
Tumor prediction  
Medical decision-making  
Finite Element Method (FEM)

## ABSTRACT

**Background and objective:** In early breast cancer diagnosis, tumor size is key to improving the patient's survival chances. It helps doctors to determine the adequate treatment for each case. Surface thermography presents encouraging results to detect thermal patterns of breast tumor abnormality. However, the early and accurate estimation of tumor size based on temperature characteristics is quite challenging due to unavailability of labeled clinical data. This work proposes a Feed-Forward Deep Neural Network (FF-DNN) for an inverse estimation of breast tumor size using thermographic data.

**Methods:** A 3D breast model was created by the COMSOL Multiphysics software incorporating tumors in the gland and covered by fat, muscle, and skin layers. Several tumor configurations are included to generate a large amount of training data. An initial thermal data analysis was performed to affirm the influence of breast tumor size on the skin surface temperature. Then, 1400 different cases were prepared, and the relevant features were extracted to train the deep learning model. The coefficient of determination ( $R^2$ ) and the Mean Square Error (MSE) were used as metrics for evaluating the predictive model.

**Results:** The analysis of the normalized temperature variations demonstrated the influence of tumor size on the surface temperature of the breast. Thus, the comparison between the FF-DNN against the Convolutional Neural Network (CNN) showed the reliability of the proposed approach. As result, the prediction accuracy indicates the capacity of the proposed FF-DNN model to estimate tumor size from the provided relevant features with an MSE value of 0.194 and an  $R^2$  value of 0.998.

**Conclusion:** The findings of this study indicate that surface thermography, when paired with deep learning, holds promise as a valuable diagnostic tool to improve the prognosis of breast cancer.

## Introduction

Breast cancer represents a terrible worldwide disease that takes the lives of women every year. The World Health Organization (WHO) reported that more than 2.3 new million breast cancer cases have been detected and approximately 685 000 deaths worldwide in 2020 [1]. Breast cancer in Morocco is the first cause of death in women and ranks as the topmost fatal disease in 2020. This year, 11 747 new breast cancer cases were diagnosed representing 38.9 % of the Moroccan women population [2]. Several factors can increase breast cancer risks such as age, family cancer history, radiation exposure history, obesity, and so many other factors [3,4]. One of the

\* Corresponding author.

E-mail address: [zakaryae.khomsi@um5s.net.ma](mailto:zakaryae.khomsi@um5s.net.ma) (Z. Khomsi).

main parameters in the prognosis of breast cancer is the tumor size. It is an important part of cancer staging. Tumor size helps doctors to determine the adequate treatment for each patient [5–7]. Small tumors can be treated with less intensive treatment than advanced-stage tumors [8,9]. Tumor size is therefore a key to improving the patient's survival chances.

Different diagnostic imaging technologies have been developed to identify breast tumors. These techniques are very helpful for medical professionals in early prevention, prognosis, and monitoring therapy [10–14]. Mammography is one of the most used techniques. It is based on X-rays imaging. During the procedure, the subject is placed in a standing position in front of the X-ray machine. Then, the breast is compressed by a plexiglass plate to obtain good screening visibility [15–17]. In general, mammography gives good results, however, it presents a risk that lies in the emission of X-rays, which are not devoid of a carcinogenic effect [18]. Thus, the compression of the breast is uncomfortable and can be painful for sensitive breasts [19].

Surface thermography serves as a supplementary screening tool [20] offering a rapid, non-invasive and cost-effective method to evaluate the surface temperature of the breast without any pain or radiation [21–23]. Breast thermal imaging, also known as a thermogram, uses modern infrared cameras to detect patterns in breast surface temperature. Malignant lesions have a higher temperature than surrounding areas, due to the hyper-vascularity resulting from the angiogenesis of cancerous tissue [24,25]. Kakileti et al. [26] discussed new advances in computer-aided diagnostics systems and thermal sensors for improving the quality of breast cancer prevention. The authors concluded that thermographic solutions hold great potential for mainstreaming this technique in early breast cancer detection over the next few years. In their survey, Singh et al. [27] outline the fundamental steps of computer-aided detection systems for breast thermography, including classification methods and features extraction. The authors recommend supplementing these methods with numerical simulation for better prediction. In their paper, Kandlikar et al. [28] examine the progress made in utilizing surface thermography for detecting breast cancer over the last thirty years. They highlight areas that still require refinement for thermal imaging to become a dependable diagnostic tool for breast cancer. The authors suggest the use of artificial neural networks, inverse modeling, and advanced simulation methods for improving the accuracy of tumor prediction.

From the literature, it is evident that surface thermography is a safe tool that has great potential for detecting the presence of breast cancer. However, the accurate estimation of tumor size based on temperature characteristics is quite challenging. Especially, real-world thermographic data of breasts with labeled tumor size are not available. For this reason, several studies used synthetic data to overcome the unavailability of labeled clinical data [29]. Synthetic data can be generated with controlled characteristics, such as tumor size, and location, allowing for controlled experiments of specific variables, conditions, or scenarios. It helps to efficiently generate large and diverse thermographic datasets with the corresponding label of tumor size that may be challenging or time-consuming to obtain from real-world sources. For example, Venkatapathy et al. [30] used a synthetic dataset containing 599 thermal images of breast models. The tumor size for each image was labeled accordingly. Then, the training was performed using machine learning (ML) models including support vector, linear, decision tree, and K-nearest neighbor regression models. The authors employed scatter plots to analyze the results and computed the mean absolute error as metric. They found that decision tree regression model (DTR) has superior predictive performance compared to other ML models. Still, a DTR model can be limited in its ability to capture complex relationships between variables, which can result in poor performance when fitting complex data. Mitra et al. [31] used synthetic data of breast thermograms in conjunction with an artificial neural network (ANN) to estimate the radius of the tumor. They generated 447 temperature data depending on the size, the location, and the heat generation rate of the tumor. The diameter of the tumor was varied from 1 to 6 mm. By evaluating the model performance, the authors adopted the neural network that predict accurately the optimal tumor parameters. Majdoubi et al. [32] proposed an inverse estimation of the tumor size by a simple FFNN. They generate 122 synthetic data cases by combining breast size, tumor size, and tumor location. Through the optimization and evaluation process, the authors proved the capacity of their trained model to predict the tumor parameters. However, the main limitations of the above-mentioned studies can be summarized as follow: (1) The lacking of thermal approximation to real breast in data generation process. Especially, the thermal combination of the biological tissues of the breast such as skin, fat, gland, and muscle are not considered in the modeling. This affects the validity of temperature data collected at steady-state conditions. (2) The low range of generated breast tumor models. Especially, the selected tumors are limited to specific cases, which does not provide a significant amount of training data. (3) The application of raw temperature data that weakly describes the temperature variations in the breast surface.

The objective of this study is to develop an FF-DNN model for the inverse estimation of breast tumor size using labeled thermographic data. Our contributions could be summarized as follow:

- (i) We improve data collection reliability through a 3D realistic breast model composed of skin, fat, gland, muscle, and tumor. Thus, we demonstrate the influence of tumor size on the breast surface temperature profile. The thermographic data collected by the COMSOL-based Finite Element Method (FEM) mimic temperature distributions on real breasts at steady-state conditions [33]. That helps make reliable decisions by the predictive model.
- (ii) We extend the tumor range. This allows a wide thermographic data collection, including various tumor possibilities. As the training data increase, the deep learning performance increases [34].
- (iii) We provide new relevant features to map the complex relationship between surface temperature and tumor size.

The remainder of the paper is organized as follows. Section 2 details our methodology from the data collection process to deep learning model formulation. In section 3, we analyzed the influence of tumor size on the surface temperature, thus, we performed a comparative analysis to evaluate the model performance. We conclude the whole study in section 4.

## Methodology

The overview of the proposed approach is shown in Fig. 1. The first step is to develop the 3D breast model and explore the surface temperature profile using COMSOL-based FEM. The second is to collect thermographic data including several tumor configurations. The next step is to prepare the dataset and extract the necessary features for training the deep learning model.

### Numerical modeling of breast cancer

The human breast is a multilayered structure composed of skin, fat, gland, and muscle. Cancer or tumor originates in different gland parts. Fig. 2 shows the approximated structure adopted for breast cancer modeling.

In living biological tissues, the heat transfer process depends on several parameters, such as metabolic heat production and blood perfusion rate. The most used mathematical model of bio-heat transfer in biological tissues is modeled by the following Pennes equation Eq (1) [35].

$$\nabla(k_L \cdot \nabla T_L) + c_b \cdot \rho_b \cdot \omega_{b,L}(T_b - T_L) + q_{m,L} = 0 \quad (1)$$

Where  $L$  represents the breast layers including skin ( $L = 1$ ), fat ( $L = 2$ ), gland ( $L = 3$ ), muscle ( $L = 4$ ), tumor ( $L = 5$ ). Thus,  $k_L$  is the thermal conductivity of the tissues,  $\omega_{b,L}$  is the blood perfusion rate of the tissues,  $T_b$  is the arterial blood temperature which is approximated by the core body temperature ( $37^\circ\text{C}$ ),  $q_{m,L}$  and  $T_L$  is respectively the metabolic heat generation rate and the temperature of each breast tissue. The density  $\rho_b$  and specific heat  $c_b$  of the blood are set at  $1060 \text{ kg/m}^3$  and  $3770 \text{ J/(kg.K)}$  respectively. Thus, the room temperature is considered equals to  $25^\circ\text{C}$  referring to low medical room temperature. The configured thermophysical properties are given in Table 1 [36–38].

To solve the bio-heat equation (1), we used the numerical modeling software COMSOL Multiphysics. The breast is modeled as a hemisphere containing the layers shown previously. The tumor is an embedded sphere in the gland. Fig. 3 illustrates the geometry and mesh of the model generated on COMSOL software.

### Surface temperature data analysis

We conducted an initial simulation under steady-state conditions. The results indicate that the presence of the tumor leads to a visible thermal gradient on the surface of the breast, as illustrated in Fig. 4.

To investigate how tumor size affects breast surface temperature, we compared temperature distributions between healthy and cancerous breasts that contained tumors of various sizes. We considered three cancer sizes,  $T1=10 \text{ mm}$ ,  $T2=20 \text{ mm}$ , and  $T3=40 \text{ mm}$ . The tumor depth is kept at  $6.6 \text{ mm}$ . Fig. 5 shows the proposed configurations. We first explored temperature distributions in the breast arc length. Then, we analyzed temperature difference between the healthy and cancerous breasts. Finally, we evaluated the normalized temperature to demonstrate the influence of tumor size on the surface breast temperature.

### Data collection

Researchers categorized cancer staging into multiple categories from small to advanced-stage tumors. The first tumor category consists of tumor sizes less than  $20 \text{ mm}$ . The second category includes tumors between  $20 \text{ mm}$  and  $50 \text{ mm}$ . The remainder categories contain tumors larger than  $50 \text{ mm}$ , which represent the advanced-stage tumors [39].

In our study, we considered a tumor range from  $2 \text{ mm}$  to  $40 \text{ mm}$  with a growth step of  $1 \text{ mm}$  included respectively in the breast model. The modeling described at section 2.1 was used to generate temperature data from numerical simulations. The simulation of these cases allows the prediction of the early-stage categories of tumors at each point of growth. Each tumor is injected randomly at approximately 40 different locations on the breast by respecting the gland wall boundaries. All possible combinations of tumor sizes and locations give us 1400 different cases of simulated models. For each case, we compiled the raw data of surface temperature by the following vector:  $T(x,y,z) = [T_{x1,y1,z1}, T_{x2,y2,z2}, \dots, T_{xM,yM,zM}]$ , with  $M = 6364$  mesh nodes elements. Every case contains temperatures information collected at the 6364 corresponding points on the surface.

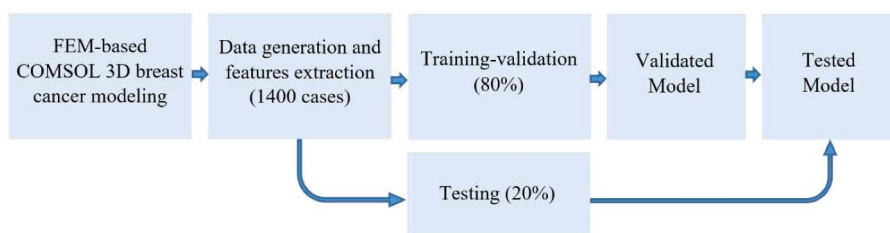
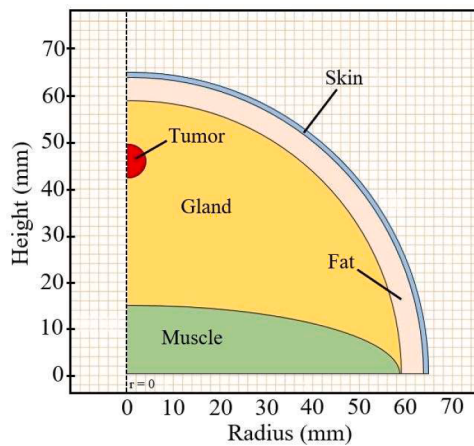


Fig. 1. Flowchart of the proposed methodology.



**Fig. 2.** Breast tissue layers used in the computational model.

**Table 1**  
Thermophysical characteristics of breast tissues.

Physical properties	Skin	Fat	Gland	Muscle	Tumor
h (mm)	1.6	5.0	43.4	15	—
k (W/m.K)	0.45	0.21	0.48	0.48	0.62
q <sub>m</sub> (W/m <sup>3</sup> )	368.1	400	700	700	70,000
ω <sub>b</sub> (mL.s <sup>-1</sup> .mL <sup>-1</sup> )	0.00018	0.00022	0.00054	0.00270	0.01600

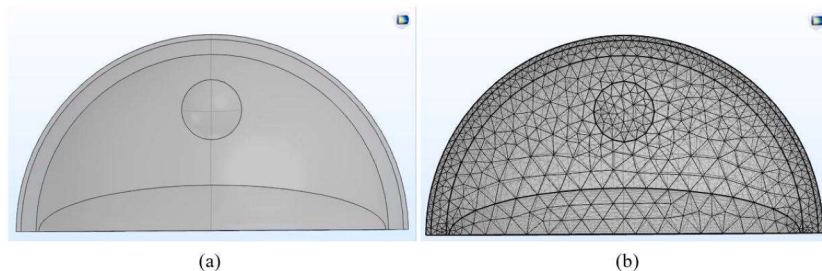


**Fig. 3.** Computational breast model: (a) Geometry section. (b) The mesh generated.

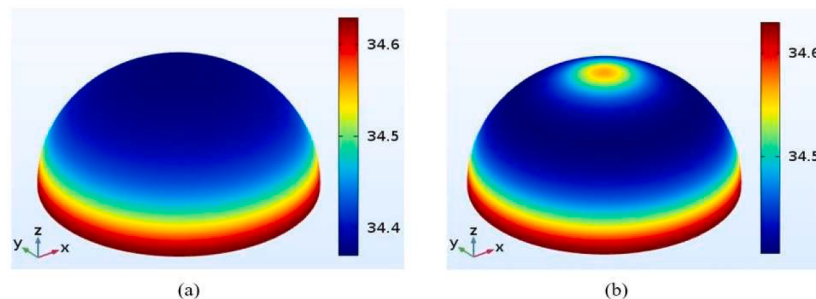


**Fig. 4.** Surface temperature of the breast: (a) without tumor. (b) with included tumor.

#### Data preparation and features extraction

First, for each tumor case, we computed the temperature variations ( $\Delta T$ ) between cancerous and healthy tissue by the following equation Eq (2). This provides a better description of the breast temperature profile.

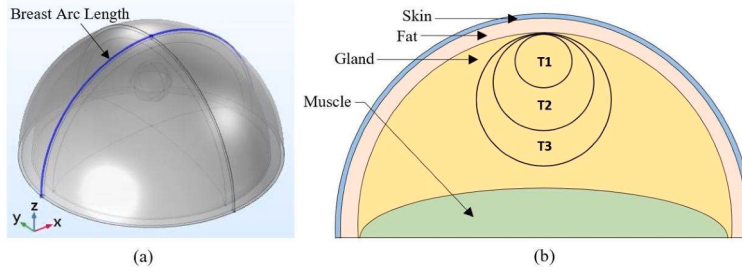


**Fig. 5.** (a) Breast arc length. (b) Tumor configurations for thermal influence analysis.

$$\Delta T(x, y, z) = T_{tumor}(x, y, z) - T_{healthy}(x, y, z) \quad (2)$$

Where,

$T_{tumor}$ : Surface temperature on breast with tumor.

$T_{healthy}$ : Surface temperature on breast without tumor.

Then, from these temperature variations, we characterized the significant information by extracting the main statistical indicators namely: Maximum variation ( $\Delta T_{max}$ ), Minimum variation ( $\Delta T_{min}$ ), Range of variation ( $\Delta T_{range}$ ), Mean of variation ( $\Delta T_{mean}$ ), Median of variation ( $\Delta T_{median}$ ), and, the Interquartile range of variation ( $\Delta T_{IQR}$ ). These parameters identify the relevant features of the tumor, which simplify the training model formulation. The final dataset consists of the 1400 cases structured according to the following format shown in Fig. 6. Thus, every sequence of the dataset contains significant information about the surface temperature profile (features) and the corresponding tumor size (target).

We normalized the input features using min-max scaling within the range [0, 1] computed by the equation Eq (3). That ensures better computational efficiency [40].

$$z_i = \frac{x_i - \text{Min}(x_i)}{\text{Max}(x_i) - \text{Min}(x_i)} \quad (3)$$

Where,  $z_i$  is the normalized value of the input value  $x_i$ .

#### Architecture of the FF-DNN model

Our proposal involved the use of an FF-DNN to predict tumor size by analyzing temperature characteristics on the surface of the breast. FF-DNN is a multi-layer network consisting of multiple hidden layers of neurons. The model receive inputs and make several processing steps (forward and backward propagation) to deliver an output.

The predictive model architecture consists of three main layers. First, the input layer contains six neurons. Each neuron represents one feature of the dataset. This layer receives the six input features ( $\Delta T_{max}$ ,  $\Delta T_{min}$ ,  $\Delta T_{range}$ ,  $\Delta T_{mean}$ ,  $\Delta T_{median}$ ,  $\Delta T_{IQR}$ ) and passes them on to the next layers. The second layer is the hidden layer that is between the input and output layers. We considered two hidden layers that consist of 64 neurons for each one. The activation function used in this layer is Rectified Linear Unit (ReLU). It will output the input directly if it is positive, else, it will output zero. It helps with easier training and often achieves better performance [41]. The third layer is the output layer. It consists of one neuron that represents the tumor size (diameter). Through the linear activation function, the model makes predictions in the output to estimate tumor size. Fig. 7 illustrates the proposed model architecture.

In forward propagation, each neuron receives a set of inputs from the previous layer and multiplies them by the corresponding weights. The weighted sum of inputs is associated with the bias of neurons and powered through the activation function to produce the neuron output. This later is passed as input to the next layer. This process is repeated for each neuron and each layer [42]. The final predicted output  $\hat{y}$  is given by the following equation Eq (4).

In the back-propagation process, the error was transmitted backward on the network. Thus, each layer's weights and biases are updated to minimize the loss function. We applied the Adam optimizer [43] to adjust these parameters with a learning rate of 0.01.

$$\hat{y} = \sum_{k=1}^l \omega_{ko} \cdot g \left( \sum_{j=1}^m \omega_{jk} \cdot g \left( \sum_{i=1}^n \omega_{ij} z_i + b_j \right) + b_k \right) \quad (4)$$

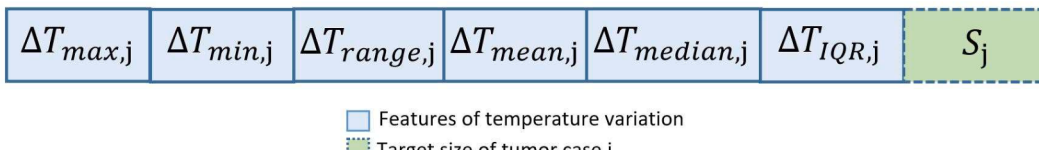


**Fig. 6.** Representative example of the final dataset format.

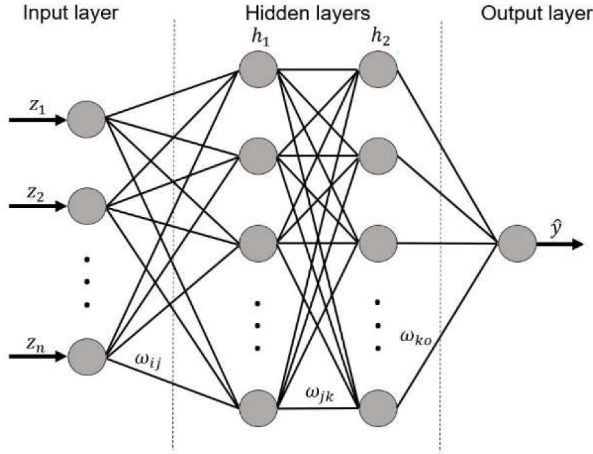


Fig. 7. Architecture of the proposed FF-DNN model.

Where,

$n$  : represents the number of neurons in the inputs layer (6 inputs);

$g$  : represents the activation function (ReLU);

$\omega_{ij}$  : is the connection weight between the  $i^{th}$  neuron of the input layer and the  $j^{th}$  neuron of the first hidden layer  $h_1$ .

$\omega_{jk}$  : is the connection weight between the  $j^{th}$  neuron of the first hidden layer  $h_1$  and the  $k^{th}$  neuron of the second hidden layer  $h_2$ .

$\omega_{ko}$  : is the connection weight between the  $k^{th}$  neuron of the second hidden layer  $h_2$  and the neuron of the output layer.

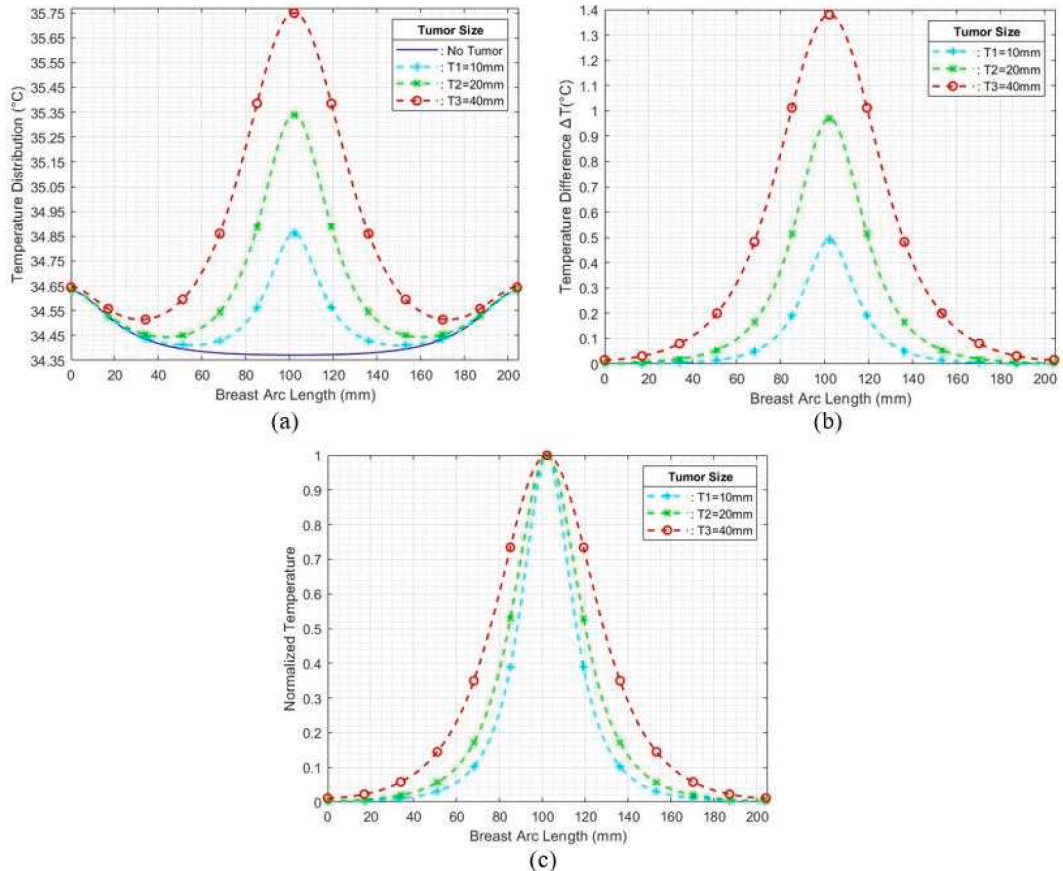


Fig. 8. Influence of tumor size: (a) Surface temperature distribution. (b) Temperature difference. (c) Normalization of temperature difference.

$m = l$  : represents the neurons number used respectively in  $h_1$  and  $h_2$  (64 Units);

$b_j$  : is the bias of the  $j^{th}$  neuron of  $h_1$ .

$b_k$  : is the bias of the  $k^{th}$  neuron of  $h_2$ .

## Results and discussion

### Tumor size influence

In this section, we investigated how tumor size affects breast surface temperature by examining tumors with diameters of 10 mm (T1), 20 mm (T2), and 40 mm (T3), all located at the same depth. Fig. 8(a) shows the temperature distribution obtained on the breast arc length. From this figure, we note that the larger size of tumor releases high temperature on the breast surface. It means that great tumors produce more heat in the breast. This makes the temperature increase on the skin surface compared to the small tumors.

Fig. 8(b) shows the computed difference in breast temperature between those with and without tumors. From the graph, we note that temperature difference achieves a maximum value as follow: 0.49( °C), 0.97( °C), and, 1.37( °C) for T1, T2, and T3 respectively. It also shows that the temperature difference increases with tumor size.

Furthermore, we evaluated the normalized temperature by dividing each temperature difference by its corresponding maximum value in the breast arc distribution. Fig. 8(c) shows the normalized temperature results. The graph indicates that the change in tumor size causes a different form of thermal perturbations on the breast surface. Therefore, these results characterize the influence of tumor size on the breast surface temperature.

### Training of the deep neural network

The training process consists of adjusting the model parameters to minimize the difference between the network's output and the desired output. We selected 1120 data samples to train the FF-DNN model, while 280 entirely different cases are prepared for testing. The training data was split randomly into 80 % for training and 20 % to validate the trained model. The training and validation process will contribute to selecting the best hyper-parameters for an accurate model. The loss function used is MSE. It measures the average squared difference between the observed and predicted values. If the model has no errors, the MSE is zero, else, its value increases as the model error increases.

We run multiple epochs at 16 batch size until the loss function converges to the global minimum. Thus, we evaluate the model's accuracy. Fig. 9 shows the obtained results.

Fig. 9(a) shows the smooth loss curves with a good fit for the model on the training and validation dataset. They indicate also a fast convergence of the neural network. Thus, Fig. 9(b) shows the gradual increases in training and validation accuracy depending on epochs until a point of stability. We note that the model achieves a good tradeoff between high accuracy and low error at 300 epochs.

### Prediction of tumor size

We adopted the trained model to test the final model performance on unseen data. The testing dataset includes tumors at new configurations on the breast model. Especially, we selected 280 different cases. Thus, we compared the predictions against the reference values. Fig. 10 shows the scatter plot obtained between the actual and predicted tumor size in millimeters. We notice that the points on the scatter plot follow a linear pattern, identifying a high linear correlation.

We evaluated the final model performance by computing the mean squared error (MSE) and the coefficient of determination ( $R^2$ ) through the equations Eq (5) and Eq (6) respectively [44].

$$MSE = \frac{1}{N} \sum_{i=1}^N (y_i - \hat{y}_i)^2 \quad (5)$$

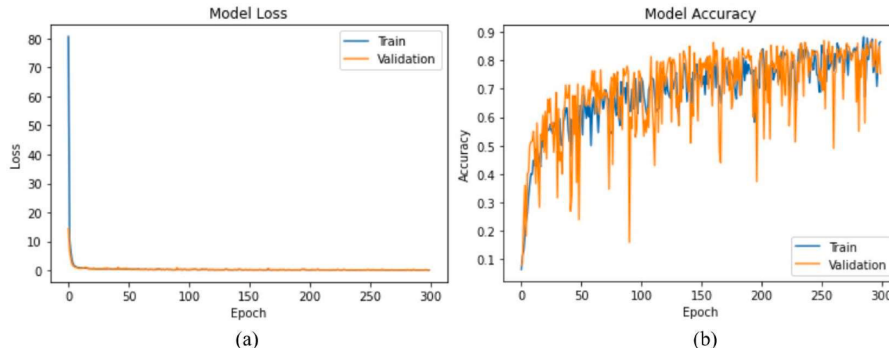
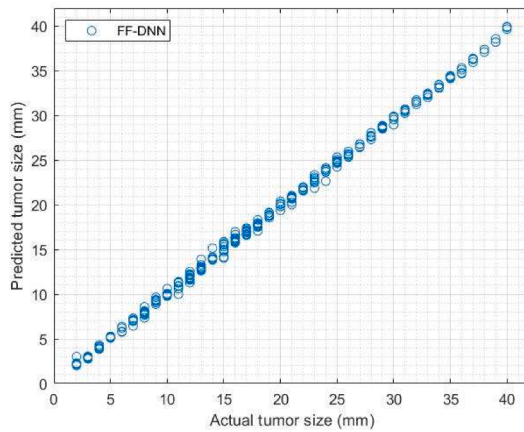


Fig. 9. Curves of the FF-DNN on the training set and validation set: (a) Model loss. (b) Model accuracy.



**Fig. 10.** Scatter plot of actual values vs predicted values of tumor size (diameter) for FF-DNN model.

$$R^2 = 1 - \frac{\sum_{i=1}^N (y_i - \hat{y}_i)^2}{\sum_{i=1}^N (y_i - \bar{y})^2} \quad (6)$$

Where  $N$  is number of examples,  $y_i$  is the actual value,  $\hat{y}_i$  is predicted value,  $\bar{y}$  is the mean of  $y_i$ .

We found an  $MSE$  of 0.194, and a coefficient of determination  $R^2$  of 0.998. The lower value obtained of  $MSE$  indicates the better predictive capability of our model. Thus, the  $R^2$  value is very close to 1 which indicates the high efficiency of the network. Furthermore, the proposed FF-DNN model is able to learn the new relevant features of the skin surface temperature and establish the correlation between the temperature distribution and the tumor size.

#### Impact of the amount of training data

The amount of training data is among the crucial elements of the deep learning model's effectiveness [45]. We considered three different numbers of samples respectively, 504, 907, and 1120. This allows the evaluation of the model performance based on different amounts of training data. The  $MSE$  obtained for different data samples is given in Fig. 11.

As illustrated in Fig. 11, the model's performance was weak when trained on 504 samples, with a large  $MSE$ . However, when the number of training samples was increased to 1120, the  $MSE$  decreased and the predictions became more accurate. Therefore, the increase in training data adds more relevant information that improves the model performance.

#### Comparative analysis

In the model development process, the comparison of deep learning models is an important step to provide insights for model selection, improvement, and benchmarking. First, we compared the proposed FF-DNN model with a CNN model which is widely used in the medical imaging field [46]. CNN has the ability to automatically learn and extract relevant features from large image datasets. In our context, we formulated a CNN model able to predict tumor size using thermographic image dataset. We exported the same 1400 tumor cases generated previously in a png image format as shown in Fig. 12. Thus, each image was labeled with the corresponding tumor size.

The CNN architecture used consists of an input layer with a shape of  $224 \times 224 \times 3$  representing an image with RGB channels. The first convolutional layer has 32 filters with a kernel size of  $3 \times 3$ , and a stride of  $2 \times 2$ . This allows the filters to move by two pixels in both the horizontal and vertical directions. The dilatation is set to  $1 \times 1$ , and padding is set to "Same" for maintaining the same spatial dimensions of the feature maps. The ReLU activation function is used in this convolutional layer, which introduces non-linearity to capture complex patterns in the data. Next, the max pooling layer with a pool size of  $2 \times 2$ , a stride of  $1 \times 1$ , and padding set to "valid" is applied to downsample the feature maps, reducing the spatial dimensions and computational complexity. The extracted features are flattened and passed through two fully connected layers each with 64 units and the ReLU activation function. Finally, the output layer uses a linear activation function to produce the final prediction of tumor size.

The thermal images dataset was randomly split into training and testing sets with a ratio of 80:20, with 1124 images used for training and 282 images for testing. Thus, we applied the Adam optimizer with a 0.0001 learning rate for adjusting parameters. The training is carried out during several epochs at 16 batch size. Fig. 13 shows the obtained results for the CNN model.

From Fig. 13(a), the CNN loss curves show the smoothness and fast convergence for both the training and testing image dataset. We notice that the CNN model achieves a good fit at 30 epochs. Fig. 13(b) shows the points on the scatter plot obtained which maintain an acceptable linear correlation. Table 2 summarizes the comparison between FF-DNN and CNN model's performance.

These results demonstrate that both FF-DNN and CNN models showed promising results in predicting tumor size from thermographic data. However, the FF-DNN model achieves superior predictive performance compared to the CNN model, as it achieved a

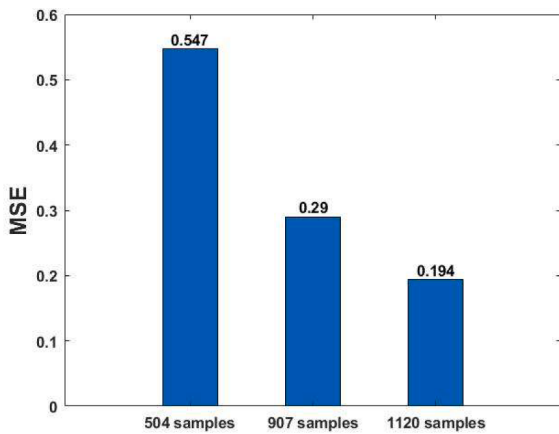


**Fig. 11.** Amount of training data impact.

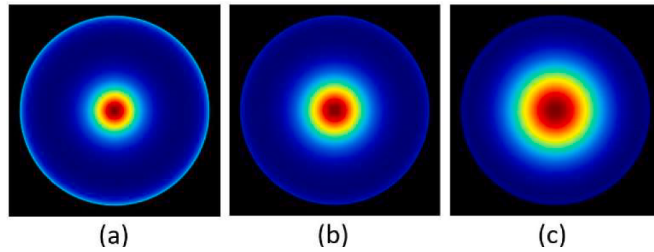


**Fig. 12.** Example of thermal images with different tumor sizes: (a) 10 mm. (b) 20 mm. (c) 40 mm.

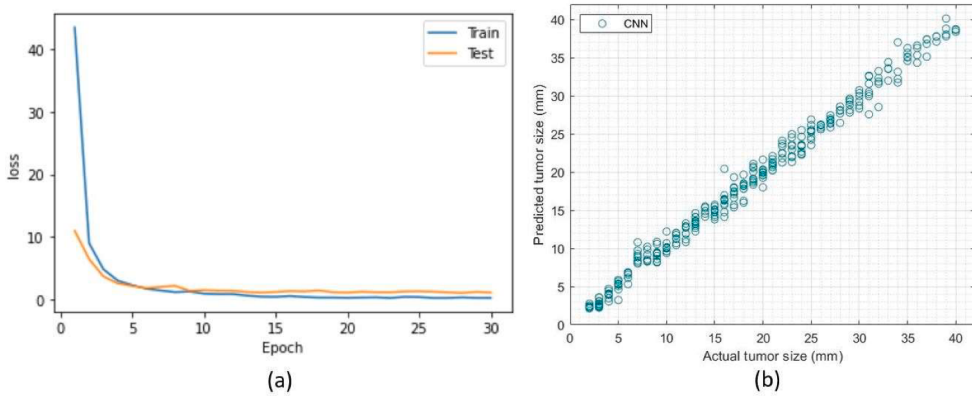


**Fig. 13.** (a) Loss curves of the CNN on the training and testing set. (b) Actual vs predicted tumor size values for CNN model.

**Table 2**

Performance of the FF-DNN and CNN models on testing data.

DL Model	R <sup>2</sup>	MSE	Training time (seconds)
FF-DNN	0.998	0.194	784
CNN	0.99	1.095	1322

higher R<sup>2</sup> and lower MSE. Thus, it is important to acknowledge that training time can be a limitation of the CNN model, as it took longer to train compared to the FF-DNN model. Nevertheless, future research can further investigate ways to optimize training time for CNN models by maintaining higher predictive accuracy.

Second, our proposed approach is also compared with different state-of-art methods as shown in Table 3.

**Table 3**

Comparison of the proposed approach with other existing methods.

Study	Dataset	Methodology	Results
Mitra et al. [31]	They generated a dataset consisting of 447 temperature data for different tumors simulated on a simplified breast model (gland)	They feed an ANN (1 hidden layer; 15 units) with raw temperature values collected from a simplified breast model to estimate the size of the tumor.	They achieved a coefficient of correlation of 0.95 (=0.902 as R <sup>2</sup> value) on testing data using ANN with raw temperature vectors
Majdoubi et al. [32]	They generated a dataset consisting of 122 cases of temperature data for limited tumors extracted from a simplified breast model (fat)	They estimated tumor size based on raw temperature points on the surface using a simple FFNN (1 hidden layer; 18 units)	They achieved an R <sup>2</sup> value of 0.933 and an MSE value of 3.578 on 7 testing samples using FFNN with raw temperature points
This study	We have generated a set of 1400 different cases of thermographic data for a wide range of tumors collected from a realistic breast model (skin, fat, gland, and muscle)	We have performed the influence analysis of tumor size on breast surface temperature. Thus, we have extracted new relevant features from temperature vectors to train the FF-DNN model (2 hidden layers; 128 units)	We have achieved a high R <sup>2</sup> value of 0.998 with a low MSE value of 0.194 on testing data using FF-DNN with new relevant features of temperature variations

The comparison of our study with the existing methods revealed several advantages. First, we generated the largest dataset using a realistic breast model, as opposed to the simplified breast models used in previous studies [31,32]. This allowed us to collect reliable simulations of thermographic data for a wide range of breast tumor models resulting in a more comprehensive and representative dataset. Second, we extracted new relevant features from raw thermographic data to train the FF-DNN model, which contributes to improving the prediction performance. Additionally, by utilizing the R<sup>2</sup>, MSE and training time metrics, we provided a more detailed and informative analysis of the deep learning model's performance, leading to a deeper understanding of the potential areas for improvement.

Furthermore, the adoption of the FF-DNN model in this study has resulted in superior predictive accuracy compared to other existing methods, underscoring the effectiveness of this approach for inverse estimation of breast tumor size using thermographic data. Consequently, the combination of a realistic breast model, new relevant features, and deep learning models represents a novel and promising approach that surpasses the limitations of existing methods.

#### *Important recommendations for future research*

After presenting our findings, it is important to acknowledge some limitations of our study. Firstly, the study utilized synthetic data due to the absence of real-world data of breast thermograms with labeled tumor size, which may not fully reflect the complexity and variability of clinical data. Therefore, the generalization of our results to real clinical settings may require careful consideration due to potential challenges.

Second, while the study proposed new relevant features, it is important to explore novel features or feature engineering techniques that could potentially improve the models' interpretability. Additionally, the study utilized a regression task for the estimation of tumor size, but further investigation into the classification of tumor stage could provide additional insights into the models' performance in different scenarios.

Lastly, the study focused on breast cancer prognosis, and future research could explore the applicability of the developed approach to other types of cancer (skin cancer) or medical conditions. Additionally, incorporating multi-modal imaging, such as combining thermographic data with other imaging modalities, could potentially improve the overall accuracy and clinical relevance of the models.

#### **Conclusion**

In this paper, we developed a deep-learning model for estimating breast tumor size using thermal data. Firstly, the COMSOL-based 3D breast model composed of skin, fat, gland, and muscle was solved by the Pennes bio-heat equation. Then, the influence of tumor sizes on the breast skin surface temperature was demonstrated through the analysis of the corresponding normalized temperatures. A large quantity of temperature data was collected at steady-state conditions including several tumor sizes and locations on the breast. Next, the final dataset was prepared and the relevant features were extracted to train the predictive model. According to the obtained results, we found that the prediction accuracy indicated the potential of the proposed FF-DNN model to estimate tumor size with an acceptable range of error. As the amount of training data increases, the deep learning model becomes more accurate. Thus, the comparative analysis indicates that the FF-DNN is more appropriate while resulting in a better tradeoff between prediction accuracy and computational efficiency compared to the CNN model. Overall, the findings of this study present a comprehensive and rigorous approach that combines a realistic breast model, novel features, and deep learning models that hold promise for enhancing the accuracy and effectiveness of breast tumor prediction using surface thermography. Moreover, our study also opens up new directions in future research, including the exploration of hybrid approaches that combine synthetic and real-world data to further improve the applicability in real-world clinical settings.

## Data availability

The data that support the findings of this study are available on request from the corresponding author.

## Declaration of Competing Interest

The authors declare that they have no known competing financial interests or personal relationships that could have appeared to influence the work reported in this paper.

## Acknowledgments

We thank Al-Khawarizmi program to encourage research in Artificial Intelligence and its applications, Rabat, Morocco.

## References

- [1] Breast cancer, (n.d.). <https://www.who.int/news-room/fact-sheets/detail/breast-cancer> (accessed February 1, 2023).
- [2] H. El Agouri, M. Azizi, H. Attar, M. Khannoussi, A. Ibrahim, R. Kabbaj, H. Kadiri, S. BekarSabein, S. EchCharif, C. Mounjid, B. Khannoussi, Assessment of deep learning algorithms to predict histopathological diagnosis of breast cancer: first Moroccan prospective study on a private dataset, *BMC Res. Notes.* 15 (2022), <https://doi.org/10.1186/s13104-022-05936-1>.
- [3] Y.S. Sun, Z. Zhao, Z.N. Yang, F. Xu, H.J. Lu, Z.Y. Zhu, W. Shi, J. Jiang, P.P. Yao, H.P. Zhu, Risk factors and preventions of breast cancer, *Int. J. Biol. Sci.* 13 (2017) 1387–1397, <https://doi.org/10.7150/ijbs.21635>.
- [4] M. Kamińska, T. Ciszewski, K. Łopacka-Szatan, P. Miota, E. Starosławska, Breast cancer risk factors, *Prz. Menopauzalny.* 14 (2015) 196–202, <https://doi.org/10.5114/pm.2015.54346>.
- [5] L. Provencher, C. Diorio, J.C. Hogue, C. Doyle, S. Jacob, Does breast cancer tumor size really matter that much? *Breast* 21 (2012) 682–685, <https://doi.org/10.1016/j.breast.2012.07.003>.
- [6] S.C. Tate, V. Andre, N. Enas, B. Ribba, I. Gueorguieva, Early change in tumour size predicts overall survival in patients with first-line metastatic breast cancer, *Eur. J. Cancer.* 66 (2016) 95–103, <https://doi.org/10.1016/j.ejca.2016.07.009>.
- [7] W.M. Sarraj, R. Tang, A.L. Najjar, M. Griffin, A.H. Bui, A. Zambeli-Ljepovic, M. Senter-Zapata, M. Lewin-Berlin, L. Fernandez, J. Buckley, A. Ly, E. Brachtel, O. Afshari, J. Gilbertson, Y. Yagi, M. Gadd, K.S. Hughes, B.L. Smith, J.S. Michaelson, Prediction of primary breast cancer size and T-stage using micro-computed tomography in lumpectomy specimens, *J. Pathol. Inform.* 6 (2015) 60, <https://doi.org/10.4103/2153-3539.170647>.
- [8] F. Fei, C. Messina, L. Slaets, C. Chakiba, D. Cameron, J. Bogaerts, H. Bonnefoi, Tumour size is the only predictive factor of distant recurrence after pathological complete response to neoadjuvant chemotherapy in patients with large operable or locally advanced breast cancers: a sub-study of EORTC 10994/BIG 1-00 phase III trial, *Eur. J. Cancer.* 51 (2015) 301–309, <https://doi.org/10.1016/j.ejca.2014.11.023>.
- [9] J.S. Michaelson, M. Silverstein, J. Wyatt, G. Weber, R. Moore, E. Halpern, D.B. Kopans, K. Hughes, Predicting the survival of patients with breast carcinoma using tumor size, *Cancer* 95 (2002) 713–723, <https://doi.org/10.1002/cncr.10742>.
- [10] D. Barba, A. León-Sosa, P. Lugo, D. Suquillo, F. Torres, F. Surre, L. Trojman, A. Caicedo, Breast cancer, screening and diagnostic tools: all you need to know, *Crit. Rev. Oncol. Hematol.* 157 (2021), <https://doi.org/10.1016/j.critrevonc.2020.103174>.
- [11] K. Loizidou, R. Elia, C. Pitris, Computer-aided breast cancer detection and classification in mammography: a comprehensive review, *Comput. Biol. Med.* 153 (2023), 106554, <https://doi.org/10.1016/j.combiomed.2023.106554>.
- [12] S. Pavithra, R. Vanithamani, J. Justin, Computer aided breast cancer detection using ultrasound images, *Mater. Today Proc.* 33 (2020) 4802–4807, <https://doi.org/10.1016/j.matpr.2020.08.381>.
- [13] E.Y.K. Ng, A review of thermography as promising non-invasive detection modality for breast tumor, *Int. J. Therm. Sci.* 48 (2009) 849–859, <https://doi.org/10.1016/j.ijthermalsci.2008.06.015>.
- [14] N. Arora, D. Martins, D. Ruggerio, E. Tousimis, A.J. Swistel, M.P. Osborne, R.M. Simmons, Effectiveness of a noninvasive digital infrared thermal imaging system in the detection of breast cancer, *Am. J. Surg.* 196 (2008) 523–526, <https://doi.org/10.1016/j.amjsurg.2008.06.015>.
- [15] F. Sardanelli, T.H. Helbich, Mammography: EU SOBI recommendations for women's information, *Insights Imaging.* 3 (2012) 7–10, <https://doi.org/10.1007/s13244-011-0127-y>.
- [16] K. Schilling, D. Narayanan, J.E. Kalinyak, J. The, M.V. Velasquez, S. Kahn, M. Saady, R. Mahal, L. Chrystal, Positron emission mammography in breast cancer presurgical planning: comparisons with magnetic resonance imaging, *Eur. J. Nucl. Med. Mol. Imag.* 38 (2011) 23–36, <https://doi.org/10.1007/s00259-010-1588-9>.
- [17] R. Murakami, N. Uchiyama, H. Tani, T. Yoshida, S. Kumita, Comparative analysis between synthetic mammography reconstructed from digital breast tomosynthesis and full-field digital mammography for breast cancer detection and visibility, *Eur. J. Radiol. Open.* 7 (2020), 100207, <https://doi.org/10.1016/j.ejro.2019.12.001>.
- [18] A. Berrington De González, G. Reeves, Mammographic screening before age 50 years in the UK: comparison of the radiation risks with the mortality benefits, *Br. J. Cancer.* 93 (2005) 590–596, <https://doi.org/10.1038/sj.bjc.6602683>.
- [19] V.A. Loving, S. Aminololama-Shakeri, J.W.T. Leung, Anxiety and Its Association with Screening Mammography, *J. Breast Imag.* 3 (2021) 266–272, <https://doi.org/10.1093/jbi/wbab024>.
- [20] J.R. Keyserlingk, P.D. Ahlgren, E. Yu, N. Belliveau, Infrared imaging of the breast: initial reappraisal using high-resolution digital technology in 100 successive cases of stage I and II breast cancer, *Breast* 4 (1998) 245–251, <https://doi.org/10.1046/j.1524-4741.1998.440245.x>.
- [21] A. Mashevko, Y. Zhao, E.Y.K. Ng, V. Zarikas, S.C. Fok, O. Mukhmetov, Early detection of the breast cancer using infrared technology – a comprehensive review, *Therm. Sci. Eng. Prog.* 27 (2022), 101142, <https://doi.org/10.1016/j.tsep.2021.101142>.
- [22] A. Lozano, F. Hassaniipour, Infrared imaging for breast cancer detection: an objective review of foundational studies and its proper role in breast cancer screening, *Infrared Phys. Technol.* 97 (2019) 244–257, <https://doi.org/10.1016/j.infrared.2018.12.017>.
- [23] R. Resmini, L. Faria da Silva, P.R.T. Medeiros, A.S. Araujo, D.C. Muchalut-Saade, A. Conci, A hybrid methodology for breast screening and cancer diagnosis using thermography, *Comput. Biol. Med.* (2021) 135, <https://doi.org/10.1016/j.combiomed.2021.104553>.
- [24] G. Kroemer, J. Pouyssegur, Tumor cell metabolism: cancer's Achilles' Heel, *Cancer Cell* 13 (2008) 472–482, <https://doi.org/10.1016/j.ccr.2008.05.005>.
- [25] H.A. Collier, Is cancer a metabolic disease? 9582978472, *Am. J. Pathol.* 184 (2014) 4–17, <https://doi.org/10.1016/j.ajpath.2013.07.035>.
- [26] S.T. Kakileti, G. Manjunath, H. Madhu, H.V. Ramprakash, Advances in breast thermography, *New Perspect. Breast Imag.* (2017), <https://doi.org/10.5772/intechopen.69198>.
- [27] D. Singh, A.K. Singh, Role of image thermography in early breast cancer detection- Past, present and future, *Comput. Methods Programs Biomed.* 183 (2020), <https://doi.org/10.1016/j.cmpb.2019.105074>.
- [28] S.G. Kandlikar, I. Perez-Ray, P.A. RaghuPathi, J.L. Gonzalez-Hernandez, D. Dabydeen, L. Medeiros, P. Phatak, Infrared imaging technology for breast cancer detection – Current status, protocols and new directions, *Int. J. Heat Mass Transf.* 108 (2017) 2303–2320, <https://doi.org/10.1016/j.ijheatmasstransfer.2017.01.086>.

- [29] H. Murtaza, M. Ahmed, N.F. Khan, G. Murtaza, S. Zafar, A. Bano, Synthetic data generation: state of the art in health care domain, *Comput. Sci. Rev.* 48 (2023), 100546, <https://doi.org/10.1016/j.cosrev.2023.100546>.
- [30] G. Venkatapathy, A. Mittal, N. Gnanasekaran, V.H. Desai, Inverse estimation of breast tumor size and location with numerical thermal images of breast model using machine learning models, *Heat Transf. Eng.* (2022) 1–19, <https://doi.org/10.1080/01457632.2022.2134081>.
- [31] S. Mitra, C. Balaji, A neural network based estimation of tumour parameters from a breast thermogram, *Int. J. Heat Mass Transf.* 53 (2010) 4714–4727, <https://doi.org/10.1016/j.ijheatmasstransfer.2010.06.020>.
- [32] J. Majdoubi, A.S. Iyer, A.M. Ashique, D.A. Perumal, Y.M. Mahrous, M. Rahimi-Gorji, A. Issakhov, Estimation of tumor parameters using neural networks for inverse bioheat problem, *Comput. Methods Programs Biomed.* 205 (2021), 106092, <https://doi.org/10.1016/j.cmpb.2021.106092>.
- [33] A.A.A. Figueiredo, H.C. Fernandes, F.C. Malheiros, G. Guimaraes, Influence analysis of thermophysical properties on temperature profiles on the breast skin surface, *Int. Commun. Heat Mass Transf.* 111 (2020), <https://doi.org/10.1016/j.icheatmasstransfer.2019.104453>.
- [34] F. Garcea, A. Serra, F. Lamberti, L. Morra, Data augmentation for medical imaging: a systematic literature review, *Comput. Biol. Med.* 152 (2023), 106391, <https://doi.org/10.1016/j.combiomed.2022.106391>.
- [35] H.H. Pennes, Analysis of tissue and arterial blood temperatures in the resting human forearm, *J. Appl. Physiol.* 1 (1948) 93–122, <https://doi.org/10.1152/jappl.1948.1.2.93>.
- [36] M. Gautherie, Thermopathology of breast cancer: measurement and analysis of in vivo temperature and blood flow, *Ann. N. Y. Acad. Sci.* 335 (1980) 383–415. [10.1111/j.1749-6632.1980.tb50764.x](https://doi.org/10.1111/j.1749-6632.1980.tb50764.x).
- [37] S. Hossain, F.A. Mohammadi, Tumor parameter estimation considering the body geometry by thermography, *Comput. Biol. Med.* 76 (2016) 80–93, <https://doi.org/10.1016/j.combiomed.2016.06.023>.
- [38] Y. Zhou, C. Herman, Optimization of skin cooling by computational modeling for early thermographic detection of breast cancer, *Int. J. Heat Mass Transf.* 126 (2018) 864–876, <https://doi.org/10.1016/j.ijheatmasstransfer.2018.05.129>.
- [39] A.E. Giuliano, J.L. Connolly, S.B. Edge, E.A. Mittendorf, H.S. Rugo, L.J. Solin, D.L. Weaver, D.J. Winchester, G.N. Hortobagyi, Breast cancer-major changes in the american joint committee on cancer eighth edition cancer staging manual, *CA, Cancer J. Clin.* 67 (2017) 290–303, <https://doi.org/10.3322/caac.21393>.
- [40] W.J. Niu, Z.K. Feng, B.F. Feng, Y.W. Min, C.T. Cheng, J.Z. Zhou, Comparison of multiple linear regression, artificial neural network, extreme learning machine, and support vector machine in deriving operation rule of hydropower reservoir, *Water (Switzerland)* 11 (2019), <https://doi.org/10.3390/w11010088>.
- [41] S. Muruganandam, R. Joshi, P. Suresh, N. Balakrishna, K.H. Kishore, S.V. Manikanthan, A deep learning based feed forward artificial neural network to predict the K-barriers for intrusion detection using a wireless sensor network, *Meas. Sensors.* 25 (2023), 100613, <https://doi.org/10.1016/j.measen.2022.100613>.
- [42] S. Wang, L. Wang, F. Jian, Projectile impact point prediction based on genetic algorithm BP neural network, *J. Phys. Conf. Ser.* (2019) 1345, <https://doi.org/10.1088/1742-6596/1345/5/052065>.
- [43] D.P. Kingma, J. Ba, Adam: a method for stochastic optimization, *CoRR.* (2014) abs/1412.6.
- [44] A.A.A. Alrashed, M.S. Gharibdousti, M. Goodarzi, L.R. de Oliveira, M.R. Safaei, E.P. Bandarra Filho, Effects on thermophysical properties of carbon based nanofluids: experimental data, modelling using regression, ANFIS and ANN, *Int. J. Heat Mass Transf.* 125 (2018) 920–932, <https://doi.org/10.1016/j.ijheatmasstransfer.2018.04.142>.
- [45] H. Chen, K. Wang, Z. Liu, H. Zhou, Surface temperature analysis and thermophysical property estimation for breast cancer by deep learning, *Numer. Heat Transf. Part A Appl.* 82 (2022) 411–427, <https://doi.org/10.1080/10407782.2022.2079298>.
- [46] S. Mutasa, S. Sun, R. Ha, Understanding artificial intelligence based radiology studies: CNN architecture, *Clin. Imag.* 80 (2021) 72–76, <https://doi.org/10.1016/j.clinimag.2021.06.033>.